Available online at www.sciencedirect.com

ScienceDirect

Mendeleev Commun., 2022, **32**, 649–651

Mendeleev Communications

1D Cu^{I} coordination polymers based on triphenylarsine and *N*,*N*′-ditopic co-ligands: synthesis, crystal structure and TADF properties

Yan V. Demyanov,[a] Marianna I. Rakhmanova,[a] Irina Yu. Bagryanskaya[b] and Alexander V. Artem'ev*[a]

[a] *A. V. Nikolaev Institute of Inorganic Chemistry, Siberian Branch of the Russian Academy of Sciences, 630090 Novosibirsk, Russian Federation. E-mail: chemisufarm@yandex.ru*

[b] *N. N. Vorozhtsov Novosibirsk Institute of Organic Chemistry, Siberian Branch of the Russian Academy of Sciences, 630090 Novosibirsk, Russian Federation*

DOI: 10.1016/j.mencom.2022.09.027

1D coordination polymers $[Cu_2I_2(AsPh_3)_2(L)]_n$ (L = 4,4′-bipyridine, pyrazine) were synthesized *via* the reaction of CuI with $AsPh_3$ and *N*,*N*′-ditopic co-ligand s L. At ambient temperature, these polymers exhibit short-lived (2.3–3.2 μs) thermally activated delayed fluorescence (TADF) with λ_{max} at 530 nm (L = 4,4′-bipyridine) and 605 nm (L = pyrazine) and quantum efficiency up to 45%.

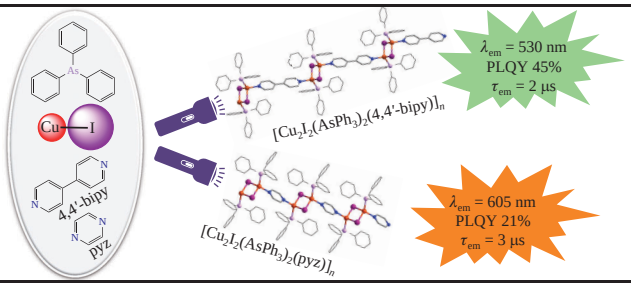

Keywords: copper(I) iodide, triphenylarsine, coordination polymers, photoluminescence, thermally activated delayed fluorescence.

Currently, luminescent Cu^{I} complexes are attracting considerable attention due to their rich structural diversity[1–4] coupled with remarkable photophysical properties such as efficient thermally activated delayed fluorescence (TADF),[5,6] room temperature phosphorescence[7] and stimuli-responsive luminescence.[8] Because of these attractive features, Cu^{I} complexes are considered now as promising emitters for energy-efficient light-emitting devices (PhOLED, TADF OLED, LEECs), sensing and bioimaging applications.[8–10] Generally, N- and P-based donating ligands are used to design Cu^{I} emitters exhibiting efficient TADF or metal-to-ligand charge transfer type phosphorescence.[5,6,11] In sharp contrast, heavier pnictine-based ligands, such as arsines, are almost unexplored in this regard,[12–16] although they show some advantages over their phosphine analogs, *e.g.*, speeding-up TADF rate at ambient temperature[17] through As-enhanced spin-orbit coupling (SOC) effect. Moreover, arsine ligands find application in catalysis, for example, in complexes of Pd(II)-catalyzed Stille coupling and Ir(III)-catalyzed dehydrogenation of cyclic hydrocarbons.[18–20] Thus, the design of new Cu^{I} complexes based on pnictine ligands is an urgent task, the solution of which can open access to new promising emissive materials with a reduced decay time. Herein, we report the synthesis and investigation of two 1D coordination polymers (CPs) $[Cu_2I_2(AsPh_3)_2(L)]_n$, **1** (L = 4,4′-bipyridine) and **2** (L = pyrazine), exhibiting bright short-lived TADF at ambient temperature. These *N*,*N*′-ditopic ligands were chosen due to their suitability for the synthesis of multimetallic complexes[21,22] and coordination polymers.[23–26]

To assemble the designed $[Cu_2I_2(AsPh_3)_2(L)]_n$ CPs, we studied the reaction of CuI with $AsPh_3$ and the above ditopic ligands L. It was found that under optimal conditions (CuI/$AsPh_3$/L molar ratio is 1 : 2 : 1.5, DMF, room temperature), CPs **1** and **2**·MeCN are formed in isolated yields of 90% and 88%, respectively. According to X-ray diffraction (XRD) analysis,† CPs **1** and **2** consist of 1D chains containing rhombic-like $[Cu_2I_2]$ fragments bridged by 4,4′-bipyridine or pyrazine ligands *via* Cu–N bonds (Figures 1 and 2). Each Cu atom is also coordinated by the $AsPh_3$ ligand, thus showing a distorted tetrahedral environment {Cu@NI$_2$As} (τ_4 = 0.98). Given that the Cu···Cu distances in the Cu_2I_2 units (*ca.* 2.8912 Å in CP **1** and 3.0397 Å in CP **2**·MeCN) are slightly longer than the twice van der Waals radius of Cu (2.80 Å), metallophilic interactions are unlikely. The distances Cu–As (average 2.37 Å), Cu–I (average 2.66 Å) and Cu–N (average 2.06 Å) in

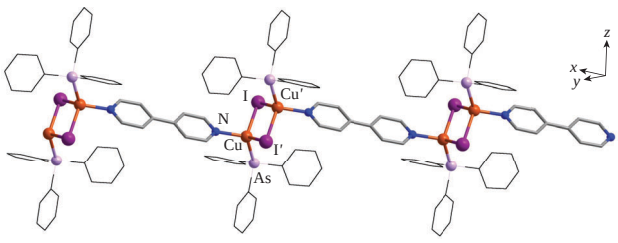

Figure 1 Fragment of 1D chain of CP **1**. H atoms are omitted for clarity, and thin lines illustrate phenyl rings. Selected bond lengths (Å): Cu···Cu′ 2.8912(6), Cu–I 2.6353(4), Cu–I′ 2.6986(4), Cu–As 2.3697(4), Cu–N 2.060(2). Symmetry code: (′) 1–*x*, 1–*y*, 2–*z*.

† *Crystal data for* **1**. $C_{23}H_{19}AsCuIN$ (M = 574.75), triclinic, space group $P\bar{1}$, a = 9.2363(4), b = 9.4311(5) and c = 13.3140(7) Å, V = 1048.14(9) Å^3, Z = 2, T = 200 K, d_{calc} = 1.821 g cm^{-3}. Total of 19337 reflections were measured, μ(MoKα) = 4.088 mm^{-1}, and 5981 independent reflections (R_{int} = 0.037) were used in the further refinement. The refinement converged to wR_2 = 0.0602 and GOF = 1.015 for all independent reflections [R_1 = 0.0275 was calculated against F for 4812 observed reflections with $I > 2\sigma(I)$].

Crystal data for **2**·MeCN. $C_{22}H_{20}AsCuIN_2$ (M = 577.76), monoclinic, space group $P2_1/n$, a = 8.9744(7), b = 18.4717(13) and c = 13.4552(9) Å, β = 94.276(3)°, V = 2224.3(3) Å^3, Z = 4, T = 200 K, d_{calc} = 1.725 g cm^{-3}. Total of 26416 reflections were measured, μ(MoKα) = 3.855 mm^{-1}, and 6492 independent reflections (R_{int} = 0.055) were used in the further refinement. The refinement converged to wR_2 = 0.1128 and GOF = 1.018 for all independent reflections [R_1 = 0.0455 was calculated against F for 3561 observed reflections with $I > 2\sigma(I)$].

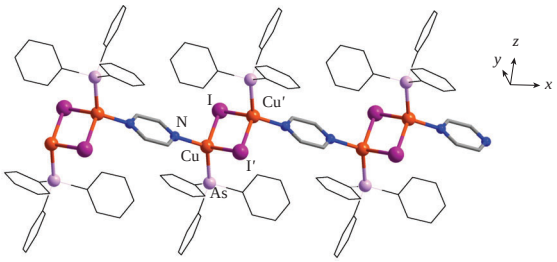

Figure 2 Fragment of 1D chain of CP **2**·MeCN. H atoms and MeCN lattice molecules are not shown, and thin lines illustrate phenyl rings. Selected bond lengths (Å): Cu···Cu′ 3.0397(11), Cu–I 2.6578(7), Cu–I′ 2.6684(7), Cu–As 2.3700(7), Cu–N 2.056(3). Symmetry code: (′) 1–*x*, 1–*y*, 1–*z*.

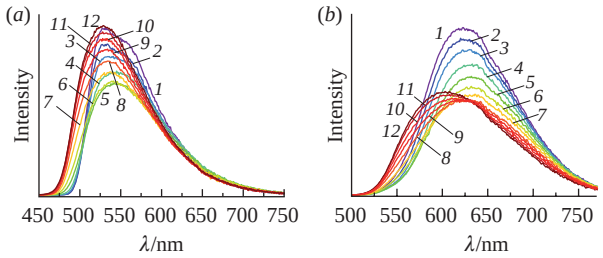

Figure 3 Temperature-dependent emission spectra of (*a*) solid CP **1** (λ_{ex} = 560 nm) and (*b*) solid CP **2**·MeCN (λ_{ex} = 625 nm), recorded at (*1*) 77, (*2*) 100, (*3*) 120, (*4*) 140, (*5*) 160, (*6*) 180, (*7*) 200, (*8*) 220, (*9*) 240, (*10*) 260, (*11*) 280 and (*12*) 300 K.

CPs **1** and **2** are comparable to the published values. Overall, the structures of the 1D chains of CPs **1** and **2**·MeCN are similar to those of their Ph_3P-derived analogs.[27,28]

Compounds **1** and **2**·MeCN are air-stable microcrystalline powders, poorly soluble in DMF, DMSO, $CHCl_3$ and CH_2Cl_2. Their phase purity was confirmed by powder XRD (Figures S1 and S2, see Online Supplementary Materials) and microanalysis data. The FTIR spectra of CPs **1** and **2**·MeCN demonstrate characteristic bands of coordinated $AsPh_3$ and L co-ligands (Figures S3 and S4), and CP **2**·MeCN features also a weak peak at 2251 cm^{-1} from the $\nu_{C\equiv N}$ vibration of MeCN solvate molecules.

Under UV irradiation at ambient temperature (298 K), CPs **1** and **2** exhibit intense solid-state photoluminescence (PL) with a quantum efficiency of 45% and 21%, respectively. Their temperature-dependent PL spectra are shown in Figure 3, and selected photophysical characteristics at 298 and 77 K are given in Table 1. As can be seen from these data, the PL spectra of CPs **1** and **2** are represented by a broad band with λ_{max} at 530 and 605 nm, respectively. Upon cooling from 298 to 77 K, the maximum of the band of CP **2** undergoes a bathochromic shift by ~20 nm, causing a pronounced change in the PL color from orange to red. At that, λ_{max} of CP **1** is shifted in red region just by ~5 nm, thus suggesting no obvious thermochromic effect. Meanwhile, when passing from 298 to 77 K, the left flank of the PL bands of both compounds gradually shifts to the long wavelength region by ~15 nm for CP **1** and ~26 nm for CP **2**, which implies TADF behavior. The broad character of emission (see Figure 3) and excitation (Figure S5) profiles of CPs **1** and **2** indicates a charge transfer character of the emission observed. In the temperature range of 77–298 K, PL decays of **1** and **2** have a monoexponential character with the remarkably short decay times at 298 K, being 2.3 and 3.2 μs, respectively. At 77 K, the PL lifetimes significantly increase to 55 μs for CP **1** and 38 μs for CP **2**, which are also noticeably short values compared to those obtained for most known Cu^I complexes at this temperature. This effect is likely associated with a higher SOC strength of arsenic (ζ_l = 1202 cm^{-1}),[32] resulting in speeding-up intersystem crossing rate process, which largely determines the overall radiative decay times. Curves of the whole temperature dependence of the decay times $\tau(T)$ of CPs **1** and **2** (Figure S6) reveal a TADF-specific shape, which indicates the manifestation of TADF at 298 K and pure phosphorescence at 77 K. Fitting the $\tau(T)$ plots with the known TADF-adapted equation (Equation S1) allowed us to evaluate the energy gaps between the lowest triplet (T_1) and singlet (S_1) excited states of CPs **1** and **2** as 1016 and 807 cm^{-1}, respectively. Both estimated $\Delta E(S_1–T_1)$ values are within the allowable range of values (< 1500 cm^{-1}) required to thermalize the S_1 level from the T_1 one at ambient temperature and thereby open the TADF channel.[5,6] Taking into account that complexes containing $[Cu_2I_2]$ generally exhibit TADF of (M+X)LCT origin (X is a halogen),[5,6,11] the TADF of the similar kind can be reasonably proposed for CPs **1** and **2**.

Table 1 Luminescence properties of solid CPs **1** and **2**·MeCN at 298 and 77 K.

Compound	λ_{max}/nm		PL decay time/μs		PLQY (%)[a]	$\Delta E(S_1–T_1)$[b]/ cm^{-1}
	298 K	77 K	298 K	77 K		
1	530	535	2.3	55	45[a]	1016
2·MeCN	605	625	3.2	38	21[b]	807

[a] Absolute PL quantum yield (PLQY) was measured at 298 K with λ_{ex} = 400 nm for CP **1** and λ_{ex} = 500 nm for CP **2**. [b] Estimated by fitting $\tau(T)$ curves (see Figure S6) with equation S1.

In summary, two previously unknown 1D CPs of $[Cu_2I_2(AsPh_3)_2(L)]_n$ type (L = 4,4′-bipyridine or pyrazine) were synthesized and structurally characterized. Temperature-dependent photophysical studies have revealed that the obtained CPs are TADF emitters with a singlet–triplet splitting on the order of 807–1016 cm^{-1} and a noticeably short decay time at ambient temperature. The presented results provide new insights into the design of efficient TADF materials with reduced lifetime.

This work was supported by the Ministry of Science and Higher Education of the Russian Federation (project nos. 121031700321-3, 121031700313-8 and 1021051503141-0-1.4.1).

Online Supplementary Materials

Supplementary data associated with this article can be found in the online version at doi: 10.1016/j.mencom.2022.09.027.

X-ray quality crystals of **1** were obtained by interlayer diffusion from DMF/MeOH/MeCN solutions. Single crystals of **2**·MeCN were crystallized using a U-shaped tube for several days. Data were collected on an automated Agilent Xcalibur diffractometer equipped with an AtlasS2 area detector [graphite monochromator, λ(MoKα) = 0.71073 Å, ω-scans]. Integration, absorption correction and determination of unit cell parameters were performed using the CrysAlisPro program package.[29] Single crystal XRD data were collected on a Bruker D8 Venture diffractometer with a CMOS PHOTON III detector and an IμS 3.0 source [mirror optics, λ(MoKα) = 0.71073 Å]. Absorption corrections were applied using the SADABS program.[30] The structures were solved by the dual space algorithm (SHELXT[31]) in the anisotropic approximation (except for H atoms). The positions of H atoms were calculated geometrically and refined in the riding model.

CCDC 2150369 and 2150370 contain the supplementary crystallographic data for this paper. These data can be obtained free of charge from The Cambridge Crystallographic Data Centre *via* http://www.ccdc.cam.ac.uk.

References

1 C. Kirst, J. Tietze, P. Mayer, H.-C. Böttcher and K. Karaghiosoff, *ChemistryOpen*, 2022, **11**, e202100224.
2 C. Lescop, *Chem. Rec.*, 2021, **21**, 544.
3 F. Moutier, J. Schiller, G. Calvez and C. Lescop, *Org. Chem. Front.*, 2021, **8**, 2893.
4 A. S. Romanov, F. Chotard, J. Rashid and M. Bochmann, *Dalton Trans.*, 2019, **48**, 15445.

5 R. Czerwieniec, M. J. Leitl, H. H. H. Homeier and H. Yersin, *Coord. Chem. Rev.*, 2016, **325**, 2.
6 H. Yersin, R. Czerwieniec, M. Z. Shafikov and A. F. Suleymanova, *ChemPhysChem*, 2017, **18**, 3508.
7 B. Huitorel, R. Utrera-Melero, F. Massuyeau, J.-Y. Mevelec, B. Baptiste, A. Polian, T. Gacoin, C. Martineau-Corcos and S. Perruchas, *Dalton Trans.*, 2019, **48**, 7899.
8 E. Cariati, E. Lucenti, C. Botta, U. Giovanella, D. Marinotto and S. Righetto, *Coord. Chem. Rev.*, 2016, **306**, 566.
9 F. Dumur, *Org. Electron.*, 2015, **21**, 27.
10 Y. Gou, M. Chen, S. Li, J. Deng, J. Li, G. Fang, F. Yang and G. Huang, *J. Med. Chem.*, 2021, **64**, 5485.
11 M. Wallesch, D. Volz, D. M. Zink, U. Schepers, M. Nieger, T. Baumann and S. Bräse, *Chem. – Eur. J.*, 2014, **20**, 6578.
12 M. F. Galimova, E. M. Zueva, A. B. Dobrynin, A. I. Samigullina, R. R. Musin, E. I. Musina and A. A. Karasik, *Dalton Trans.*, 2020, **49**, 482.
13 R. Kobayashi, R. Inaba, H. Imoto and K. Naka, *Bull. Chem. Soc. Jpn.*, 2021, **94**, 1340.
14 M. F. Galimova, E. M. Zueva, A. B. Dobrynin, I. E. Kolesnikov, R. R. Musin, E. I. Musina and A. A. Karasik, *Dalton Trans.*, 2021, **50**, 13421.
15 R. Kobayashi, H. Imoto and K. Naka, *Eur. J. Inorg. Chem.*, 2020, 3548.
16 R. Kobayashi, H. Kihara, T. Kusukawa, H. Imoto and K. Naka, *Chem. Lett.*, 2021, **50**, 382.
17 A. V. Artem'ev, Y. V. Demyanov, M. I. Rakhmanova and I. Yu. Bagryanskaya, *Dalton Trans.*, 2022, **51**, 1048.
18 T. Korenaga, A. Ko, K. Uotani, Y. Tanaka and T. Sakai, *Angew. Chem., Int. Ed.*, 2011, **50**, 10703.
19 D. F. Brayton, P. R. Beaumont, E. Y. Fukushima, H. T. Sartain, D. Morales-Morales and C. M. Jensen, *Organometallics*, 2014, **33**, 5198.
20 A. Chishiro, M. Konishi, R. Inaba, T. Yumura, H. Imoto and K. Naka, *Dalton Trans.*, 2022, **51**, 95.
21 A. A. Titov, O. A. Filippov, A. F. Smol'yakov, A. A. Averin and E. S. Shubina, *Mendeleev Commun.*, 2021, **31**, 170.
22 L. P. M. Green, T. R. Steel, M. Riisom, M. Hanif, T. Söhnel, S. M. F. Jamieson, L. J. Wright, J. D. Crowley and C. G. Hartinger, *Front. Chem.*, 2021, **9**, 786367.
23 B.-I. Bratanovici, A. Nicolescu, S. Shova, I.-A. Dascălu, R. Ardeleanu, V. Lozan and G. Roman, *Res. Chem. Intermed.*, 2020, **46**, 1587.
24 B. I. Kharisov, P. Elizondo Martínez, V. M. Jiménez-Pérez, O. V. Kharissova, B. Nájera Martínez and N. Pérez, *J. Coord. Chem.*, 2010, **63**, 1.
25 C. Pettinari, A. Tăbăcaru, I. Boldog, K. V. Domasevitch, S. Galli and N. Masciocchi, *Inorg. Chem.*, 2012, **51**, 5235.
26 N. Portolés-Gil, O. Vallcorba, C. Domingo, A. López-Periago and J. A. Ayllón, *Inorg. Chim. Acta*, 2021, **516**, 120132.
27 H. Araki, K. Tsuge, Y. Sasaki, S. Ishizaka and N. Kitamura, *Inorg. Chem.*, 2005, **44**, 9667.
28 L. Yang, D. R. Powell and R. P. Houser, *Dalton Trans.*, 2007, 955.
29 *CrysAlisPro 1.171.38.46, Data Collection, Reduction and Correction Program*, Rigaku Oxford Diffraction, 2015.
30 *Bruker APEX3 software suite: APEX3, SADABS-2016/2 and SAINT, version 2018.7-2*, Bruker AXS Inc., Madison, WI, 2017.
31 G. M. Sheldrick, *Acta Crystallogr., Sect. A: Found. Adv.*, 2015, **71**, 3.
32 M. Montalti, A. Credi, L. Prodi and M. T. Gandolfi, *Handbook of Photochemistry*, 3rd edn., CRC Press, Boca Raton, FL, 2006.

Received: 28th March 2022; Com. 22/6839